Joint Optimization for Covert Communications in UAV-Assisted NOMA Networks

Dan Deng, *Senior Member, IEEE,* Shuping Dang, *Member, IEEE,*
Xingwang Li, *Senior Member, IEEE,* Derrick Wing Kwan Ng, *Fellow, IEEE,*
and Arumugam Nallanathan, *Fellow, IEEE*

***Abstract*—In this paper, we investigate the design of the trajectory of an unmanned aerial vehicle (UAV) and the transmit power of ground users to improve covert communications against a flying warden in UAV-assisted non-orthogonal multiple access networks, where the legitimate UAV can simultaneously collect the messages from the multiple ground users in a secure manner. Taking the channel uncertainty into account, we derive the analytical expressions of the optimal normalized detection threshold, the minimum detection error probability (DEP), and the security-guaranteed transmit power constraint for the ground users that are exploited to ensure a high DEP at the warden UAV. Subsequently, the design to maximize the average covert achievable rate (CAR) subject to the constraints of flight speed, initial and final locations, transmit power, and detection performance is formulated as a non-convex optimization problem. To obtain a high-quality solution to the design problem at hand, an iterative block coordinate descent-based successive convex approximation method is proposed. From the theoretical analysis, we find that a greater channel estimation uncertainly or a lower effective received power ratio at the warden UAV is beneficial in enhancing the system covertness towards the warden UAV. Moreover, when the successful detection probability of the warden UAV is sufficiently small, the maximum effective received power ratio is linearly and positively correlated to the detection success probability. Besides, extensive simulations are presented to verify the covert performance advantages brought by the proposed method.**

***Index Terms*—Covert communications, joint optimization, NOMA, UAV-assisted communications**

I. Introduction

DUE to the openess of wireless systems, communication security is facing ever-increasing challenges nowadays [1]. In recent years, covert communications, which can prevent wireless signals from being detected by an illegitimate warden, have been adopted as an alternative viable technology for the enhancement of data security. Besides, covert communication is more practical and robust than traditional physical layer security. Considering a finite number of available channels, the pioneering work in [2] proved the fundamental limit imposing by the square root law on covert communications with a large detection error probability (DEP). In particular, continuously transmitting bits over a sufficiently long duration could lead to an error-free detection of useful information at the warden. Fortunately, with the help of noisy measurement at the illegitimate warden [3], a positive secrecy rate can still be achieved asymptotically, enabling covert communications that go beyond the square root law. Inspired by this, authors in [4] investigated the unbounded uncertainty model in terms of the average covert outage probability. Furthermore, by deriving the theoretical expressions on the optimal detection threshold and achievable outage rate region of the legitimate link, the effect of channel uncertainty on the covert achievable rate (CAR) was analyzed in [5]. Also, by exploiting the variation of wireless channel fading, channel inversion power control (CIPC) algorithm was proposed in [6], [7] to adapt the transmit power to the reciprocal of the channel power such that they significantly outperform the fixed power scheme in terms of achievable covert throughput. Besides, in cooperative networks, Y. Su proposed a relay selection scheme in [8] to enhance the covertness and demonstrated its gains in terms of CAR. To further unlock the potential of covert communications, recent literature focuses on the amalgamation of emerging technologies and covert communications, such as cognitive radio [9], backscatter communications [10], intelligent reflecting surface (IRS) [11]–[13], faster-than-Nyquist transmission [14], unmanned aerial vehicle (UAV), etc.

Among these technologies, UAV is appealing due to its high maneuverability. With the support of UAV as a novel communication paradigm, covert capacity of UAV-assisted networks can be improved from various perspectives [15], [16]. For example, for enhancing the transmission secrecy against the warden UAV, a multi-hop relaying model was investigated and a optimization problem on the number of hops was proposed in [17]. Besides, without the location knowledge of the warden, the authors in [18] focused on the millimeter-wave beam design by exploiting the stochastic minimization-maximization algorithm. Furthermore, considering the location estimation error of the warden, an iterative trajectory optimization method was proposed in [19], which can efficiently improve the covert rate. Moreover, extending from the two-dimensional (2D) to the three-dimensional (3D) UAV placement, the optimal horizontal location as well as the optimal height were analyzed

Dan Deng is with School of Information Engineering, Guangzhou Panyu Polytechnic, Guangzhou, 410630, China (e-mail: dengdan@ustc.edu).

Shuping Dang is with Department of Electrical and Electronic Engineering, University of Bristol, Bristol BS8 1UB, UK (e-mail: shuping.dang@bristol.ac.uk).

Xingwang Li is with School of Physics and Electronic Information Engineering, Henan Polytechnic University, Jiaozuo, 454150, China (e-mail: lixingwangbupt@gmail.com).

Derrick Wing Kwan Ng is with School of Electrical Engineering and Telecommunications, University of New South Wales, Sydney, NSW 2052, Australia (e-mail: w.k.ng@unsw.edu.au).

Arumugam Nallanathan is with the School of Electronic Engineering and Computer Science, Queen Mary University of London, London E1 4NS, UK (e-mail: a.nallanathan@qmul.ac.uk).

Corresponding author: Xingwang Li.

in [20], demonstrating that the 3D deployment achieves better covertness than the 2D counterpart. In addition, considering the existence of multiple potential wardens and by employing artificial noise, a joint design on the trajectory and user scheduling scheme was formulated as in [21], and a penalty convex optimization approach was developed to solve it. Also, by adopting Gaussian signaling, a covertness enhancement strategy was introduced in [22] for space-air-ground networks to minimize the covert outage probability. Furthermore, against a flying warden, Gaussian signaling transmission scheme was adopted in [23] to increase the channel uncertainty, where the variance of the Gaussian signaling as well as the transmitter's block length are jointly optimized in the worst scenario. A joint optimization algorithm on the flying heights, transmit power, and channel allocation was proposed in [24] showing a remarkable performance gain of the proposed algorithm.

Meanwhile, NOMA, which can share the spectrum among multiple users and improve resource allocation fairness, has been adopted in enabling reliable communications [25] or covert communications to hide the transmission of private messages [26]. For instance, device-to-device covertness in NOMA networks was evaluated in [27] by adopting a cellular base station as a friendly jammer. In particular, by a proper design on the transmit power, the covert capacity can be enhanced significantly. Moreover, by jointly optimizing the beamforming coefficients and the transmission power of IRS, the average error probability was derived in [28] for the downlink and uplink NOMA covert communications, showing that NOMA is indeed beneficial in guaranteeing strictly positive covert rates. Also, antenna selection algorithm was adopted in [29] to improve the covertness of the system. Combining NOMA with CIPC, a near-optimal covertness scheme was proposed in [30], [31], which can achieve considerable gains compared with single-user scenarios. Besides, L. Tao investigated the uplink NOMA covert communications in [32] coexisting with an energy harvesting jammer and revealed the optimal resource allocation scheme to maximize the CAR. Furthermore, X. Hou, et al. proposed a federated learning based covert communication framework for UAV-enabled networks in [33], where the trajectory, the power of the artificial noise and the network resources are jointly optimized to minimize the energy and the time cost.

Although the existing literature has investigated various enabling technologies and resource optimization for UAV or NOMA-assisted covert communications, few works have yet focused on the covertness in UAV-assisted NOMA networks. Indeed, the maneuverability of UAV can be exploited to enhance the communication covertness while the NOMA protocol is effective for improving the system throughput. Furthermore, the above advantages can be fully exploited by the considered UAV-assisted NOMA networks to enhance the system covert communications. Yet, the combination of NOMA and UAV in covert communications introduces novel design challenges. First, the time-varying position of the legitimate UAV could alter its distances from the warden as well as that from the target users. Meanwhile, the interference between multiple users also varies accordingly, which affects the average CAR significantly. Second, the design of the transmit power scheme for the uplink users in NOMA networks has a significant impact on the warden's received power as well as the legitimate UAV's uplink CAR. Therefore, the covert communications in UAV-assisted NOMA networks calls for a novel joint design on both the trajectory and the users' transmission power scheme.

Motivated by the aforementioned discussion, we investigate the covert communications in UAV-assisted NOMA networks by the joint optimization of the trajectory of a legitimate UAV and the transmit power of multiple ground users. In the considered scenario, the legitimate UAV collects data from multiple ground users through the uplink NOMA protocol. Meanwhile, it transmits jamming signals to protect the ground users' signals from being detected by a warden UAV. In the worst case that the warden UAV is always able to select the optimal threshold to decide whether the ground users are transmitting signals or not, we analytically derive a constraint on the transmit power of the ground users for guaranteeing a certain level of covertness. Based on this, we formulate the corresponding joint parameters design as a non-convex optimization considering communication covertness and propose an iterative block coordinate descent (BCD)-based successive convex approximation (SCA) method to obtain an effective solution to it. Please note that conventional physical layer security only focuses on the channel capacity of eavesdropping links [34], while the covert communication investigates the detection probability at the eavesdropping nodes of determining whether the legitimate links are transmitting signals or not. Therefore, compared with conventional physical layer security, covert communication is more secure and reliable in protecting private data. Moreover, UAV-enabled covert communication has been investigated in recent literature. For example, only one ground user was scheduled for the uplink transmission in [21], and the unscheduled users were treated as potential illegitimate wardens with static locations. In addition, the authors in [35] investigated the power allocation algorithm for a downlink two-user NOMA covert communication and derived the detection error probability of a static warden. In contrast, this paper focuses on the uplink multi-user NOMA covert communication against a flying warden and extends the application scenarios from perfect channel estimation to imperfect channel state information. The contributions of this paper are listed as follows:

- Under the constraints of the UAV's flight speed, initial and final locations, users' transmit power, and total DEP at the warden in UAV-assisted NOMA networks, we formulate an optimization problem to maximize the average CAR against a flying warden considering the existence of channel uncertainty.
- Considering the worst case when the warden UAV adopts the optimal detector, we derive the optimal normalized detection threshold, the overall DEP at the warden UAV, and the constraint on the transmit power of the ground users for maintaining a desired DEP at the flying warden.
- To tackle the formulated non-convex optimization problem, an iterative BCD method is employed. First, we optimize the transmit power scheme given a fixed UAV

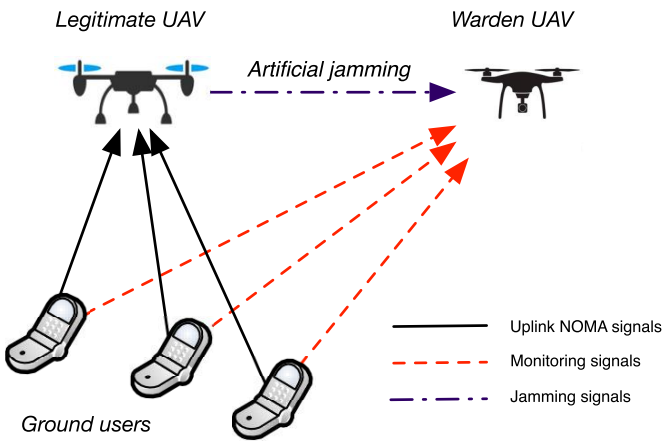

Fig. 1. Covert communications in UAV-assisted NOMA networks with a legitimate UAV, a warden UAV, and K ground users.

trajectory. Then, the trajectory of the legitimate UAV is optimized with a fixed transmit power scheme. By iterating both processes alternetingly, the trajectory and the transmit power scheme returned by the proposed method are expected to converge to an effective solution.

II. System Model

As shown in Fig. 1, the considered UAV-assisted NOMA network in this paper consists of one legitimate UAV, one passive warden UAV, and K ground users. Similar with [21], we assume that the legitimate UAV flies from the initial location $\mathbf{c}_{\rm I}$ to the final location $\mathbf{c}_{\rm F}$ at a fixed altitude $H_{\rm L}$, while the flight altitude of the warden UAV is $H_{\rm W}$. Besides, the position of the warden UAV can be obtained at the legitimate UAV by the global positioning system (GPS) or certain radar systems [34], [36]. The warden UAV always monitors the radio signal strength in the target network and decides if the ground users are transmitting any information signals. Moreover, we assume that both the ground users and the warden UAV are single-antenna devices[1], and the legitimate UAV operates in the full duplex mode and is able to collect the uplink messages from the ground users with its receive antenna while sending the jamming signals with its transmit antenna [21]. To confuse the warden UAV, the legitimate UAV continuously transmits an artificial jamming signal with fixed power $p_{\rm L}$ to cover the signals transmitted from the ground users. In addition, the artificial jamming signal can also be exploited to convey public and dedicated messages to the ground users, depending on the specific scenarios.

The static Cartesian coordinates of the kth user are denoted by $\mathbf{w}_k = (x_k, y_k)^T, \forall k$, and the maximum transmit power is $p_{\rm M}$. For simplicity, the continuous trajectories are equally divided into N slots. The time period of a single slot can be given by $T_s = \frac{T}{N}$, where T is the time period of the trajectories. The horizontal coordinates of the trajectories of the legitimate UAV and the warden UAV in the nth slot are denoted as $\mathbf{c}_{\rm L}[n] = (x_{\rm L}[n], y_{\rm L}[n])^T$ and $\mathbf{c}_{\rm W}[n] = (x_{\rm W}[n], y_{\rm W}[n])^T, \forall n$, respectively. The wireless channels between the legitimate UAV or the warden to the ground users are commonly modeled by LoS, since the altitudes of the UAVs are high enough to ensure the existence of LoS propagation paths with a high probability [34]. By adopting the NOMA protocol, taking into account the constraints of the DEP at the warden UAV, the ground users aim to improve the uplink average CAR at the legitimate UAV. Furthermore, the receiver employing perfect SIC is assumed to be adopted by the legitimate UAV, which is also widely adopted in recent literature, e.g. [28], [31]. Thus, the received self-interference from its own transmitter at the legitimate UAV can be perfectly canceled.

In the nth slot, the distances from the kth user and the legitimate UAV as well as that to the the warden UAV are determined as

$$\begin{cases} d_{{\rm L},k}[n] &= \sqrt{|\mathbf{w}_k - \mathbf{c}_{\rm L}[n]|^2 + H_{\rm L}^2}, \\ d_{{\rm W},k}[n] &= \sqrt{|\mathbf{w}_k - \mathbf{c}_{\rm W}[n]|^2 + H_{\rm W}^2}, \\ d_{\rm LW}[n] &= \sqrt{|\mathbf{c}_{\rm W}[n] - \mathbf{c}_{\rm L}[n]|^2 + (H_{\rm L} - H_{\rm W})^2}, \end{cases} \tag{1}$$

respectively. The legitimate UAV flies from its initial location $\mathbf{c}_{\rm I}$ to the final location $\mathbf{c}_{\rm F}$ along an optimized trajectory, i.e.,

$$\mathbf{c}_{\rm L}[1] = \mathbf{c}_{\rm I} \text{ and } \mathbf{c}_{\rm L}[N] = \mathbf{c}_{\rm F}. \tag{2}$$

Also, the speed of the legitimate UAV should satisfy the following constraint:

$$|\mathbf{c}_{\rm L}[n+1] - \mathbf{c}_{\rm L}[n]| \le V_m T_s, \forall n, \tag{3}$$

where V_m is the maximum flight speed of the legitimate UAV. We assume that the ground users are sorted in an ascending order of the distance from the legitimate UAV, i.e.,

$$d_{{\rm L},i}[n] \le d_{{\rm L},j}[n], \text{if } i < j, \forall n. \tag{4}$$

As studied in [38], when the UAV's flying altitude exceeds 40 m, the channel fading coefficients of the UAV follow the LoS fading model almost surely, which has been also adopted in recent literature, e.g., [35], [39]. In addition, the classical NOMA protocol is adopted by the ground users in the uplink channels. Therefore, in the nth slot, the received signal at the legitimate UAV is

$$\begin{aligned} r_{\rm L}[n] &= \sum_{k=1}^{K} \left(h_{{\rm L},k}[n] \sqrt{p_k[n]} x_k[n] \right) + v_{\rm L}[n] \\ &= \sum_{k=1}^{K} \left(\sqrt{\frac{\beta p_k[n]}{d_{{\rm L},k}^2[n]}} x_k[n] \right) + v_{\rm L}[n], \end{aligned} \tag{5}$$

where $h_{{\rm L},k}[n] = \sqrt{\frac{\beta}{d_{{\rm L},k}^2[n]}}$ denotes the the wireless channel fading coefficient from the kth user to the legitimate UAV; $\beta > 0$ indicates the wireless channel power fading coefficient at the standard reference distance, i.e., $d = 1$ m; $p_k[n]$ denotes the uplink transmit power of the kth user; $x_k[n] \in \mathbb{C}$ is the transmitted symbol from the kth user with a normalized mean power $E(|x_k[n]|^2) = 1$; $v_{\rm L}[n] \sim \mathcal{CN}(0, \sigma^2)$ is the AWGN received at the legitimate UAV, and σ^2 denotes its variance.

Considering that the downlink broadcast channel and its associated pilot signal are continuously transmitted by the

[1]The single-antenna model is widely adopted in recent literature, e.g., [34], [37]. Furthermore, adopting the multi-antenna model will be investigated in the future work.

legitimate UAV, a MMSE channel estimator [40] is assumed to be adopted for exploiting the received pilot at the warden to acquire the channel state information (CSI) of the illegitimate link from the legitimate UAV to the warden, i.e., $h_{\mathrm{WL}}[n]$. Besides, similar processing methods can also be adopted by the legitimate UAV for the uplink signals to obtain the CSI of the ground users. Moreover, considering the path loss introduced by the LoS channel as given in (5), the transmit power of the ground users can also be obtained by the legitimate UAV. Due to the noisy environment, there exists an estimation error $\tilde{h}_{\mathrm{WL}}[n]$, which is uncorrelated with the accurate CSI $h_{\mathrm{WL}}[n]$. In particular, the elements of $\tilde{h}_{\mathrm{WL}}[n]$ follow independent zero-mean complex Gaussian distribution. Similar assumptions have also been widely adopted in recent literature [5], [41]. The detailed channel uncertainty model will be discussed in the following sections.

III. Performance Analysis

Covert communications can be evaluated under two hypotheses [12], [42]. Specifically, because the warden UAV always listens to the wireless signals along its trajectory, in the nth time slot, the received signal at the warden UAV can be represented by

$$r_{\mathrm{W}}[n]=\begin{cases} h_{\mathrm{WL}}[n]\sqrt{p_{\mathrm{L}}}x_{\mathrm{L}}[n]+v_{\mathrm{W}}[n], & H_0,\\ h_{\mathrm{WL}}[n]\sqrt{p_{\mathrm{L}}}x_{\mathrm{L}}[n]+ \\ \sum_{k=1}^{K}\left(h_{\mathrm{W},k}[n]\sqrt{p_k[n]}x_k[n]\right)+v_{\mathrm{W}}[n], & H_1, \end{cases} \tag{6}$$

where p_{L} is the fixed transmit power of the continuous artificial jamming signal at the legitimate UAV, $x_{\mathrm{L}}[n]\in\mathbb{C}$ is the transmitted symbol from the legitimate UAV with a normalized mean power $E(|x_{\mathrm{L}}[n]|^2)=1$ [2], $h_{\mathrm{W},k}[n]=\sqrt{\frac{\beta}{d^2_{\mathrm{W},k}[n]}}$ and $h_{\mathrm{W}L}[n]=\sqrt{\frac{\beta}{d^2_{\mathrm{L}W}[n]}}$ denote the channel fading coefficients of the warden UAV from the kth ground user and the legitimate UAV, respectively; $v_{\mathrm{W}}[n]\sim\mathcal{CN}(0,\sigma^2)$ is the AWGN received at the warden UAV. Hypothesis H_0 denotes the event that only the legitimate UAV is transmitting a jamming signal, while H_1 denotes that both the legitimate UAV and the users are transmitting their own messages simultaneously. Note that with the help of an encrypted pilot signal that is confidential to the warden UAV, $x_{\mathrm{L}}[n]$ can also be exploited to convey public and dedicated messages to the ground users [44], [45]. With the help of the global positioning system (GPS) or certain radar systems, the position information of both the warden UAV and the ground users can be obtained by the legitimate UAV. Therefore, the CSIs for both the legitimate and the illegitimate links, i.e., $\{h_{\mathrm{WL}}[n],h_{\mathrm{L},k}[n]\}$, can be calculated according to the LoS channel models described in (5) and (6), respectively. It's worthing mentioning that, these assumptions regarding the channel acquisition and the position of the warden at the legitimate UAV have been widely adopted in recent literature, such as [34], [36].

[2]Compared with the time-varying transmit power scheme for the artificial jamming signal as in [21], [43], the fixed transmit power scheme for p_{L} at the legitimate UAV is simpler to implement. Besides, $x_{\mathrm{L}}[n]$ is a fast time-varying modulated signal with a constant envelope, such that the artificial jamming signal cannot be easily filtered out by the warden.

A. Channel Uncertainty Model

It is assumed that the MMSE estimator is adopted by the receiver of the warden UAV [5], [41]. Therefore, the estimation of the channel fading coefficient by the warden UAV can be modeled as

$$\hat{h}_{\mathrm{WL}}[n]=\sqrt{\alpha}h_{\mathrm{WL}}[n]+\sqrt{1-\alpha}\tilde{h}_{\mathrm{WL}}[n], \tag{7}$$

where α denotes the correlation factor of the channel estimation, $\hat{h}_{\mathrm{WL}}[n]$ is the estimation of $h_{\mathrm{WL}}[n]$, and $\tilde{h}_{\mathrm{WL}}[n]\sim\mathcal{CN}(0,h^2_{\mathrm{WL}}[n])$ characterizes the channel uncertainty. Specifically, in most of the application scenarios, we can assume that $0.5\leq\alpha\leq 1$. Also, the estimation error model is applied on $h_{\mathrm{W},k}[n]$.

The average wireless power received at the warden can be estimated through downlink pilot by the following equation

$$\hat{E}_{\mathrm{W}}[n]=\left[\frac{1}{M}\sum_{m=1}^{M}\left(r_{m,\mathrm{W}}[n]*\hat{h}^{*}_{m,\mathrm{WL}}[n]\right)\right]^2, \tag{8}$$

where $r_{m,\mathrm{W}}[n]$ denotes the mth sample of $r_{\mathrm{W}}[n]$ in the nth slot, and $\hat{h}_{m,\mathrm{WL}}[n]$ is the associated mth estimated version of $h_{\mathrm{WL}}[n]$. Thus, if M is sufficiently large, by substituting (6) and (7) into (8), we can obtain the normalized long-term observation of the warden's wireless power detector [29]

$$E_{\mathrm{W}}[n]=\begin{cases}\alpha p_0[n]+(1-\alpha)p_0[n]u_0+\sigma^2, & H_0,\\ \alpha p_1[n]+(1-\alpha)p_1[n]u_1+\sigma^2, & H_1,\end{cases} \tag{9}$$

where $p_0[n]=\frac{\beta p_{\mathrm{L}}}{d^2_{\mathrm{WL}}[n]}$, $p_1[n]=p_0[n]+\sum_{k=1}^{K}\frac{\beta p_k[n]}{d^2_{\mathrm{W},k}[n]}$, u_0 and u_1 follow the standard exponential distribution, i.e., $u_0,u_1\sim\exp(x,1)$, with

$$\exp(x,\lambda)=\begin{cases}\lambda e^{-\lambda x}, & \text{if } x\geq 0,\\ 0, & \text{if } x<0.\end{cases} \tag{10}$$

According to (9), when the perfect CSI is assumed, i.e., $\alpha=1$, the warden can accurately distinguish the two hypotheses almost surely through the long-term observations. As such, only the case of $\alpha<1$ needs to be considered. Moreover, we assume that the value of α can be obtained perfectly by the legitimate UAV, which can be achieved through training with the help of *Theorem* 1. For example, in the training phase, the ground user continuously adjusts its transmit power while the legitimate UAV observes the alarm probability of the warden UAV such that the value of α can be calculated by (18).

B. Detection Performance at the Warden

With a predefined threshold $\tau[n]$, according to the following criterion, the warden UAV makes a decision on whether the ground users are transmitting signals or not:

$$E_{\mathrm{W}}[n]\underset{D_0}{\overset{D_1}{\gtrless}}\tau[n]. \tag{11}$$

Then, the false alarm probability P_{FA} and the missed detection probability P_{MD} can be written as

$$\begin{aligned}P_{\mathrm{FA}}&=\Pr\{D_1|H_0\}\\&=\Pr\{\alpha p_0[n]+(1-\alpha)p_0[n]u_0+\sigma^2>\tau[n]\},\end{aligned} \tag{12}$$

and

$$\begin{aligned} P_{\mathrm{MD}} &= \Pr\{D_0|H_1\} \\ &= \Pr\{\alpha p_1[n] + (1-\alpha)p_1[n]u_1 + \sigma^2 < \tau[n]\}, \end{aligned} \tag{13}$$

respectively. Therefore, the overall DEP can be determined as

$$P_{\mathrm{E}} = P_{\mathrm{FA}} + P_{\mathrm{MD}}. \tag{14}$$

The warden UAV always tries to reduce its DEP by selecting the optimal predefined threshold τ. Given the definition of the ratio of the received power from the ground users at the warden UAV to that of the legitimate UAV [3]

$$\eta[n] = \frac{p_1[n] - p_0[n]}{p_0[n]} = \frac{\sum_{k=1}^{K} \frac{\beta p_k[n]}{d^2_{\mathrm{W},k}[n]}}{\frac{\beta p_{\mathrm{L}}}{d^2_{\mathrm{LW}}[n]}}, \tag{15}$$

and the normalized threshold

$$\hat{\tau}[n] = \frac{\tau[n] - \sigma^2}{(1-\alpha)p_0}, \tag{16}$$

we have the following theorem and corollaries.

Theorem 1 *The optimal normalized threshold and the minimum overall DEP at the warden UAV are*

$$\hat{\tau}^*[n] = \begin{cases} c_1(1+\eta[n]), & \text{if } \alpha \geq 0.5, \\ \frac{1+\eta[n]}{\eta[n]} \ln(1+\eta[n]), & \text{if } \alpha < 0.5, \end{cases} \tag{17}$$

and

$$P_{\mathrm{E,min}}[n] = \begin{cases} e^{-c_1\eta[n]}, & \text{if } \alpha \geq 0.5, \\ 1 - e^{c_1} T(\eta[n]), & \text{if } \alpha < 0.5, \end{cases} \tag{18}$$

respectively, where

$$\begin{cases} c_1 = \frac{\alpha}{1-\alpha}, \\ T(x) = x(1+x)^{-(1+\frac{1}{x})}. \end{cases} \tag{19}$$

Proof *See Appendix A.* [4] ■

Corollary 1 *$T(x)$ is a monotonically increasing function with respect to (w.r.t.) x and $P_{\mathrm{E,min}}[n]$ is monotonically decreasing w.r.t. $\eta[n]$ and α, respectively.*

Proof *See Appendix B.* ■

Remark 1: According to *Corollary* 1, we can see that a larger correlation factor α leads to a lower minimum DEP $P_{\mathrm{E,min}}[n]$. The reason for this phenomenon is that the larger the correlation factor, the smaller the interference introduced by the MMSE estimator at the warden UAV, which inevitably improves the successful detection probability. As a consequence, $P_{\mathrm{E,min}}[n]$ will be raised.

Remark 2: In each time slot, a lower $\eta[n]$ is of benefit to increase $P_{\mathrm{E,min}}[n]$ of the warden. The reason is that a lower $\eta[n]$ means a smaller difference of the effective received power under the two hypotheses, which increases the detection difficulty of the warden UAV.

Corollary 2 *By applying* Theorem *1 and* Corollary *1, to satisfy the overall DEP constraint, i.e., $P_{\mathrm{E,min}} > 1-\delta$, the maximum value of $\eta[n]$ is*

$$\eta^* = \begin{cases} \frac{1}{c_1} \ln \frac{1}{1-\delta}, & \text{if } \alpha \geq 0.5, \\ T^{-1}(\delta e^{-c_1}), & \text{if } \alpha < 0.5. \end{cases} \tag{20}$$

We note that the above equation indicates the constraint of the received power ratio in the nth slot, and the corresponding insights are summarized in the below remarks.

Remark 3: According to the expression on the maximum power ratio η^* in (20), η^* is monotonically increasing w.r.t. the detection success probability δ. The explanation for the above phenomenon is that a higher η^* allows a higher transmit power of the ground users, and is obviously helpful to improve the detection success probability δ.

Remark 4: Since η^* is a monotonically decreasing w.r.t. c_1 while c_1 is monotonically increasing w.r.t. the correlation factor α, η^* is monotonically decreasing w.r.t. α. The reason is that a larger correlation factor α can reduce the interference introduced by the MMSE estimator at the warden UAV, which leads to a lower DEP. To guarantee a tolerable DEP at the warden UAV, the legitimate UAV should raise its transmit power or the ground user should reduce its transmit power. which results in a lower power ratio η^*.

Corollary 3 *Given $\delta \to 0$, the asymptotic expression on the maximum power ratio η^* is*

$$\eta^* \to \begin{cases} \frac{\delta}{c_1}, & \text{if } \alpha \geq 0.5, \\ \delta e^{1-c_1}, & \text{if } \alpha < 0.5. \end{cases} \tag{21}$$

Proof *See Appendix C.* ■

Remark 5: According to *Corollary* 3, when δ is sufficiently small, the maximum power ratio η^* is linearly and positively correlated to δ.

Thus, by substituting (20) into (15), we obtain the following constraint on the transmit power of the ground users to ensure a desired level of the DEP at the warden UAV

$$\sum_{k=1}^{K} \frac{p_k[n]}{d^2_{\mathrm{W},k}[n]} \leq \eta^* \frac{p_{\mathrm{L}}}{d^2_{\mathrm{LW}}[n]}, \forall n. \tag{22}$$

Moreover, due to the cost and volume limitations of the mobile user equipment, $p_k[n]$ should also meet the maximum constraint, i.e.,

$$p_k[n] \leq p_{\mathrm{M}}, \forall n, k, \tag{23}$$

where p_{M} is the maximum transmit power of the ground users.

C. Average CAR

Considering the uplink CAR, it is assumed that SIC receiver is adopted at the legitimate UAV. According to the NOMA protocol, the SIC receiver decodes different users' data in descending order of the received power [28]. Thus, considering

[3] Please note that $\eta[n]$ denotes the ratio of the additional received power from the ground users to that of the public signal. The fundamental constraints of $\eta[n]$ can provide a direct guidance for the design of key parameters such as the transmission power and coverage radius for covert communication in UAV-assisted NOMA networks.

[4] c_1 denotes the ratio of the correlated term of the estimated CSI in (7) to that of the uncorrelated term, while $T(\cdot)$ is a user-defined transcendental function, which will be discussed thoroughly in the following sections.

the received signal at the legitimate UAV as in (5), the SNR of the kth user is

$$\gamma_k[n] = \frac{\frac{\beta p_k[n]}{d^2_{\mathrm{L},k}[n]}}{\sum_{j=k+1}^{K} \frac{\beta p_j[n]}{d^2_{\mathrm{L},j}[n]} + \sigma^2}, \forall n, k. \tag{24}$$

Therefore, the CAR of the kth user can be calculated as

$$R_k[n] = B \log_2(1 + \gamma_k[n]), \tag{25}$$

where B is the bandwidth of the networks. Then, the average CAR of the legitimate UAV along its trajectory can be determined as

$$R = \frac{1}{N} \sum_{n=1}^{N} \sum_{k=1}^{K} R_k[n]. \tag{26}$$

IV. Problem Formulation and Solution

Our objective for covert communications is to maximize the average CAR while guaranteeing a tolerable minimum DEP at the warden UAV. To improve the average CAR, the legitimate UAV needs to carefully design its trajectory. Since the uplink NOMA protocol is adopted, the transmit power of the ground users should be coordinated to achieve the maximum uplink sum rate. Generally, the power control commands can be computed and sent from the legitimate UAV to the users through the dedicated downlink control channels. The joint optimization design can be formulated as

$$\text{(P0)}: \max_{\mathbf{P}, \mathbf{c}_\mathrm{L}} R \tag{27}$$

$$s.t.\ \ (2), (3), (22), (23), \tag{27a}$$

where $\mathbf{P} = \{p_k[n], \forall n, k, \}$ denotes the transmit power scheme of the ground user, and $\mathbf{c}_\mathrm{L} = \{\mathbf{c}_\mathrm{L}[n], \forall n, \}$ represents the trajectory of the legitimate UAV. Since $p_k[n]$ and $\mathbf{c}_\mathrm{L}[n]$ are coupled in the objective function R and constraint (22), the problem (P0) is non-convex and challenging to solve.

To tackle the formulated problem, the iterative BCD-based SCA method is adopted to obtain an effective suboptimal solution to problem (P0). Specifically, we first optimize the transmit power scheme $p_k[n]$ with a fixed UAV trajectory $\mathbf{c}^r_k[n]$ and a local solution $p^r_k[n]$. Second, the optimal trajectory of the legitimate UAV $\mathbf{c}_\mathrm{L}[n]$ is obtained with a fixed transmit power scheme $p_k[n]$ and a local solution $\mathbf{c}^r_\mathrm{L}[n]$. After several rounds of iterative optimization, the trajectory and transmit power scheme are convergent to a solution to problem (P0).

A. Transmit Power Optimization

With a fixed UAV trajectory, by using SCA method, we present the solution to the optimal transmit power of the users. As defined in (25) and (24), $R_k[n]$ is non-convex w.r.t. $p_k[n]$. Fortunately, we can rely on the following lemma to proceed with the analysis:

Lemma 1 *For any positive real-valued a, b and x, $\ln(a + \frac{x}{b})$ is a concave function and $\ln(a + \frac{b}{x})$ is a convex function.*

Proof *See Appendix D.* ■

Given the following definitions

$$\begin{cases} S_k[n] & = \sum_{j=k}^{K} \frac{p_j[n]}{d^2_{L,j}[n]} + \frac{\sigma^2}{\beta}, \text{if } k \in [1, K-1], \\ S_{K+1} & = \frac{\sigma^2}{\beta}, \end{cases} \tag{28}$$

the CAR of the kth user $R_k[n]$ as defined in (25) can be determined as

$$\begin{aligned} R_k[n] &= \frac{B}{\ln 2} \ln \left(1 + \frac{\frac{\beta p_k[n]}{d^2_{L,k}[n]}}{\sum_{j=k+1}^{K} \frac{\beta p_j[n]}{d^2_{L,j}[n]} + \sigma^2} \right) \\ &= \frac{B}{\ln 2} (\ln S_k[n] - \ln S_{k+1}[n]). \end{aligned} \tag{29}$$

By introducing a set of auxiliary optimization variables $\hat{R}_k[n]$, (29) can be lower bounded by

$$\ln S_k[n] - \ln S_{k+1}[n] \geq \hat{R}_k[n], \forall n, k. \tag{30}$$

Thus, with a fixed trajectory, the subproblem on the transmit power scheme can be formulated as

$$\text{(P1)}: \max_{p_k[n], \hat{R}_k[n]} \frac{B}{\ln 2} \sum_{k=1}^{K} \hat{R}_k[n] \tag{31}$$

$$\text{s.t.}\ \ (22), (23), (30). \tag{31a}$$

According to *Lemma* 1, both $\ln S_k[n]$ and $\ln S_{k+1}[n]$ are concave w.r.t. $p_k[n]$. We use $p^r_k[n]$ to denote the local solution in the rth iteration. With a feasible point $p^r_k[n]$, by using the first-order Taylor series expansion, $\ln(S_{k+1}[n])$ can be upper bounded by

$$\begin{aligned} \ln\left(S_{k+1}[n]\right) \leq & \ln S^r_{k+1}[n] \\ & + \frac{1}{S^r_{k+1}[n]} \sum_{j=k+1}^{K} \frac{(p_j[n] - p^r_j[n])}{d^2_{\mathrm{L},j}[n]}, \end{aligned} \tag{32}$$

where $S^r_k[n] = \sum_{j=k}^{K} \frac{p^r_j[n]}{d^2_{\mathrm{L},j}[n]} + \frac{\sigma^2}{\beta}$. Specifically, the equation in (32) holds if and only if the optimized solution equals the local solutioin, i.e., $p_j[n] = p^r_j[n]$. Thus, a subset of (30) is solved by

$$\begin{aligned} \ln S_k[n] - \hat{R}_k[n] \geq & \ln S^r_{k+1}[n] \\ & + \frac{1}{S^r_{k+1}[n]} \sum_{j=k+1}^{K} \frac{(p_j[n] - p^r_j[n])}{d^2_{\mathrm{L},j}[n]}, \forall n, k. \end{aligned} \tag{33}$$

With the local solution $p^r_k[n]$, a lower bound of (P1) can be obtained by solving

$$\text{(P2)}: \max_{p_k[n], \hat{R}_k[n]} \frac{B}{\ln 2} \sum_{k=1}^{K} \hat{R}_k[n], \forall n, \tag{34}$$

$$\text{s.t.}\ \ (22), (23), (33). \tag{34a}$$

Obviously, the objective function in (P2) is affine w.r.t. $\hat{R}_k[n]$, (22) and (23) are linear constraints w.r.t. $p_k[n]$, and (33) is convex w.r.t. $\hat{R}_k[n]$ and $p_k[n]$. Therefore, it is proved that (P2) is convex. Given a fixed UAV trajectory $\mathbf{c}^r_\mathrm{L}$ and a local solution $p^r_k[n]$ in rth iteration, (P2) can be solved by standard convex optimization tools [46]. Furthermore, the classical SCA method [47] can be used to further tighten the bound in (P2) and improve the solution to (P1). The details of the

optimization algorithm for (P1) with a fixed UAV trajectory are presented in Algorithm 1. Specifically, under the constraints in (22) and (23), the initial value of $p_k^0[n]$ can be obtained with the maximum feasible values by adopting the equal transmit power mode at the ground users.

We note that the difference between (P1) and (P2) is the the constraints on $p_k[n]$ in (30) and (33). Since the constraint in (33) is more stringent than that of (30), the solution to (P2) is also feasible to (P1). On the other hand, since the objective value in Algorithm 1 is non-decreasing over iterations and the solution set is compact, it is guaranteed that Algorithm 1 converges after s sufficient number of iterations [39].

Algorithm 1 Transmit Power Optimization for (P1)

1: **input** : Given a fixed UAV trajectory $\mathbf{c}_{\mathrm{L}}^r[n]$.
2: **initialize** Set the iteration index $r = 0$; set the initial transmit power scheme $p_k^0[n], \forall k$ with the maximum feasible values by using equal power transmit mode; set the convergence threshold $\xi > 0$; calculate the objective function $Y^r[n] \triangleq \frac{B}{\ln 2}\sum_{k=1}^{K}\hat{R}_k[n]$ in (34).
3: **repeat**
4: With given trajectory $\mathbf{c}_{\mathrm{L}}^r[n]$ and a local transmit power solution $p_k^r[n]$, apply CVX to solve problem (P2) in (34), and obtain the solution $p_k^{r+1}[n]$ for each time slot.
5: Use $p_k^{r+1}[n]$ and $\mathbf{c}_{\mathrm{L}}^r[n]$ to update the objective function $Y^{r+1}[n]$.
6: Update $r \leftarrow r+1$.
7: **until** The relative difference of the objective function is not greater than ξ, i.e., $\frac{Y^{r+1}[n]-Y^r[n]}{Y^r[n]} \le \xi$.
8: **output** : $\{p_k[n], \forall n, k.\}$

B. Trajectory Optimization

With the given transmit power scheme of the ground users $p_k[n]$, under the constraints of the flight speed, we try to obtain the solution to the optimal trajectory, which leads to the maximum average CAR. The subproblem given transmit power scheme is formulated by

$$\text{(P3)}: \max_{\mathbf{c}_{\mathrm{L}}[n],\hat{R}_k[n]} \frac{B}{N\ln 2}\sum_{n=1}^{N}\sum_{k=1}^{K}\hat{R}_k[n] \tag{35}$$

$$\text{s.t. } (2),(3),(22),(30). \tag{35a}$$

Since the constraints in (2) and (3) are linear and convex, respectively, our effort is devoted to addressing constraints (22) and (30) such that they are convex w.r.t. $\mathbf{c}_{\mathrm{L}}[n]$. Substituting (1) into (22), we obtain the following convex constraint on $\mathbf{c}_{\mathrm{L}}[n]$:

$$(H_{\mathrm{L}}-H_{\mathrm{W}})^2 + |\mathbf{c}_{\mathrm{L}}[n]-\mathbf{c}_{\mathrm{W}}[n]|^2 \le \frac{\eta^* p_{\mathrm{L}}}{\sum_{k=1}^{K}\frac{p_k[n]}{d_{\mathrm{W},k}^2[n]}}, \forall n. \tag{36}$$

According to *Lemma* 1, $y = \ln\left(a + \frac{b}{H^2+|\mathbf{c}_{\mathrm{L}}[n]-\mathbf{w}_k|^2}\right)$ is convex w.r.t. $(H^2+|\mathbf{c}_{\mathrm{L}}[n]-\mathbf{w}_k|^2)$, while non-convex and non-concave w.r.t. $\mathbf{w}_k$. [5] In the tth iteration, with the help of a local solution $\mathbf{c}_{\mathrm{L}}^t[n]$, by performing the first-order Taylor series expansion on $\ln S_k[n]$ w.r.t. $H_{\mathrm{L}}^2+|\mathbf{c}_{\mathrm{L}}[n]-\mathbf{w}_j|^2$, we obtain

$$\ln S_k[n] \ge \ln S_k^t[n] - \frac{1}{S_k^t}\sum_{j=k}^{K}\frac{p_j[n]X_j[n]}{(H_{\mathrm{L}}^2+|\mathbf{c}_{\mathrm{L}}^t[n]-\mathbf{w}_j|^2)^2}, \tag{37}$$

where

$$S_k^t = \sum_{j=k}^{K}\frac{p_j[n]}{H_{\mathrm{L}}^2+|\mathbf{c}_{\mathrm{L}}^t[n]-\mathbf{w}_j|^2} + \frac{\sigma^2}{\beta}, \tag{38}$$

and

$$X_j[n] = (|\mathbf{c}_{\mathrm{L}}[n]-\mathbf{w}_j|^2 - |\mathbf{c}_{\mathrm{L}}^t[n]-\mathbf{w}_j|^2). \tag{39}$$

Moreover, by performing the first-order approximation on $X_j[n]$ w.r.t. $\mathbf{c}_{\mathrm{L}}[n]$, we obtain

$$X_j[n] \ge 2(\mathbf{c}_{\mathrm{L}}^t[n]-\mathbf{w}_j)^T(\mathbf{c}_{\mathrm{L}}[n]-\mathbf{c}_{\mathrm{L}}^t[n]) \triangleq Y_j[n]. \tag{40}$$

Considering the second term of (30), in a similar manner, the approximation as in [34] can be obtained as follows:

$$\ln S_{k+1} \ge \ln S_{k+1}^t - \frac{1}{S_{k+1}^t}\sum_{j=k+1}^{K}\frac{p_j[n]Y_j[n]}{(H_{\mathrm{L}}^2+|\mathbf{c}_{\mathrm{L}}^t[n]-\mathbf{w}_j|^2)^2}. \tag{41}$$

By the results derived in (37) and (41), (30) can be rewritten as

$$\ln S_k^t - \frac{1}{S_k^t}\sum_{j=k}^{K}\frac{p_j[n]X_j[n]}{(H_{\mathrm{L}}^2+|\mathbf{c}_{\mathrm{L}}^t[n]-\mathbf{w}_j|^2)^2} \ge \hat{R}_k[n] + \ln S_{k+1}^t - \frac{1}{S_{k+1}^t}\sum_{j=k+1}^{K}\frac{p_j[n]Y_j}{(H_{\mathrm{L}}^2+|\mathbf{c}_{\mathrm{L}}^t[n]-\mathbf{w}_j|^2)^2}. \tag{42}$$

Since $X_j[n]$ is convex and $Y_j[n]$ is linear, the convexity of (42) is thereby proved.

Thus, in the tth iteration, given a fixed transmit power scheme $p_k[n]$ and a local solution $\mathbf{c}_{\mathrm{L}}^t[n]$, subproblem (P3) can be approximated as

$$\text{(P4)}: \max_{c_{\mathrm{L}}[n],\hat{R}_k[n]} \frac{B}{N\ln 2}\sum_{n=1}^{N}\sum_{k=1}^{K}\hat{R}_k[n] \tag{43}$$

$$\text{s.t. } (2),(3),(36),(42). \tag{43a}$$

Since all the constraints are convex w.r.t. $\mathbf{c}_{\mathrm{L}}[n]$ and affine w.r.t. $\hat{R}_k[n]$ while the objective function is affine w.r.t. $\hat{R}_k[n]$, the problem in (P4) is convex. As a consequence, the SCA method can also be used to obtain an lower bound solution to problem (P3). The details of the optimization method are given in Algorithm 2.

C. Joint Optimization Algorithm

Overall, by introducing the iterative BCD method, we can handle the original problem in (P0) by solving the transmit power problem in (P2) and the trajectory problem in (P4) alternatingly. The details of the joint optimization algorithm for (P0) are given in Algorithm 3. The BCD algorithm can

[5] Please note that $\mathbf{w}_k$ denotes the static Cartesian coordinates of the kth ground user, which is defined in Section II.

Algorithm 2 UAV Trajectory Optimization for (P3)

1: **input** : Given a fixed transmit power scheme $\{p_k^r[n], \forall k, n\}$.
2: **initialize** Set the iteration index $t = 0$; set the initial trajectory $\mathbf{c}_{\mathrm{L}}^t[n]$ with a uniform straight line model; set the convergence threshold $\xi > 0$; calculate the objective function $Z^t = \sum_{n=1}^{N} \sum_{k=1}^{K} \hat{R}_k^t[n]$.
3: **repeat**
4: With given transmit power solution $p_k^r[n]$ and a local solution $\mathbf{c}_{\mathrm{L}}^t[n]$, adopt CVX to solve problem (P4) in (43), and obtain the solution $\mathbf{c}_{\mathrm{L}}^{t+1}[n]$.
5: Use $p_k^r[n]$ and $\mathbf{c}_{\mathrm{L}}^{t+1}[n]$ to update the objective function Z^{t+1}.
6: Update iteration index $t \leftarrow t + 1$.
7: **until** The relative difference of the objective function is not greater than ξ, i.e., $\frac{Z^{t+1} - Z^t}{Z^t} \leq \xi$.
8: **output** : The optimized variables $\{\mathbf{c}_{\mathrm{L}}^{t+1}[n], \forall n\}$.

decompose coupled optimization problems into several simple uncoupled subproblems. Specifically, by using classic convex optimization tools, it is possible to obtain the solution to the simple subproblems and finally converge to the solution to the original problem alternatingly. Since (P0) is difficult to be solved directly, the BCD algorithm can be adopted to obtain its solution efficiently. Also, it has been used in recent literature, such as [34], [48]. We note that since the Taylor approximation is adopted in (32) and (37), we can obtain a local optimal solution for (P0) [39].

Algorithm 3 Joint Trajectory and Transmit Power Optimization for (P0)

1: **initialize** : Set the iteration index with $r = 0$; set the initial trajectory $\{\mathbf{c}_{\mathrm{L}}^r[n], \forall n\}$ with a uniform rectilinear model; set the initial transmit power scheme $\{p_k^0[n], \forall k\}$ with the maximum feasible values by using equal power transmit mode; set the convergence threshold $\xi > 0$; and calculate the objective function R^r.
2: **repeat**
3: With a given trajectory $\mathbf{c}_{\mathrm{L}}^r[n]$ and a local transmit power solution $p_k^r[n]$, apply CVX to solve the transmit power optimization problem in (P1) by Algorithm 1, and obtain the solution $p_k^{r+1}[n]$ for each time slot.
4: With the updated power scheme $p_k^{r+1}[n]$ and a local trajectory solution $\mathbf{c}_{\mathrm{L}}^r[n]$, apply CVX to solve the trajectory optimization problem in (P3) by Algorithm 2, and obtain the solution $\mathbf{c}_{\mathrm{L}}^{r+1}[n]$.
5: Use $p_k^{r+1}[n]]$ and $\mathbf{c}_{\mathrm{L}}^{r+1}[n]$ to calculate the updated objective function R^{r+1}.
6: Update iteration index $r \leftarrow r + 1$.
7: **until** The relative difference of the objective function is not greater than ξ, i.e., $\frac{R^{r+1} - R^r}{R^r} \leq \xi$.
8: **output** : $\{\mathbf{c}_{\mathrm{L}}[n], p_k[n], \forall n, k.\}$

Moreover, in each iteration of Algorithm 3., the objective function is non-decreasing, i.e., $R^{r+1} \geq R^r$. On the other hand, the average CAR is a bounded function. Moreover, the relative difference between the objective function returned by two adjacent iterations needs to be not greater than a predefined threshold ξ. Thus, Algorithm 3 is convergent.

The computational complexity of Algorithm 3 is jointly determined by the iteration number, the variables' number as well as the desired convergence accuracy. Following [49], since the number of variables is $3NK+N$, the computational complexity can be estimated as

$$\chi = \mathcal{O}\big((3NK + N)^{3.5} \ln(1/\xi)\big) \cdot I, \tag{44}$$

where the definition of $\mathcal{O}(\cdot)$ is given as $f = \mathcal{O}(g)$, if $\lim_{n\to\infty} \frac{f(n)}{g(n)} = C, C > 0$, and I is the iteration number of Algorithm 3.

V. Simulation Results

Numerical results are presented to evaluate the effectiveness and efficiency of the proposed joint trajectory and power optimization algorithm. In our setup, four ground users, one legitimate UAV, and one warden UAV are distributed over a 300 m $\times$ 300 m square area. The system parameter configurations are detailed as follows: the wireless channel power fading coefficient at the reference distance is $\beta = 10^{-6}$; the number of the slots is $N = 40$; the time duration of each slot is $T_s = 2$ s; the system bandwidth is $B = 10$ MHz; the received AWGN power is $\sigma^2 = -110$ dBm; the convergence threshold of Algorithm 1 is $\xi = 10^{-3}$; the locations of users are $[0, 0]^T, [0, 100]^T, [100, 0]^T, [100, 100]^T$; the altitude of the legitimate UAV is $H_{\mathrm{L}} = 100$ m; the maximum speed of the legitimate UAV is $V_m = 20$ m/s; similar with the setup in [42], the transmit power of the legitimate UAV is $p_{\mathrm{L}} = 2500$ mW; the initial location and the final location of the legitimate UAV are $\mathbf{c}_{\mathrm{I}} = [0, 0]^T$ and $\mathbf{c}_{\mathrm{F}} = [300, 300]^T$, respectively; the flight altitude of the warden UAV is $H_{\mathrm{W}} = 150$ m; the initial location and the final location of the warden UAV are $\mathbf{c}_{\mathrm{W,I}} = [250, 0]^T$ and $\mathbf{c}_{\mathrm{W,F}} = [0, 250]^T$, respectively; the correlation factor of the channel estimation at the warden UAV is $\alpha = 0.6$, the overall detection success probability threshold at the warden UAV is $\delta = 0.05$.

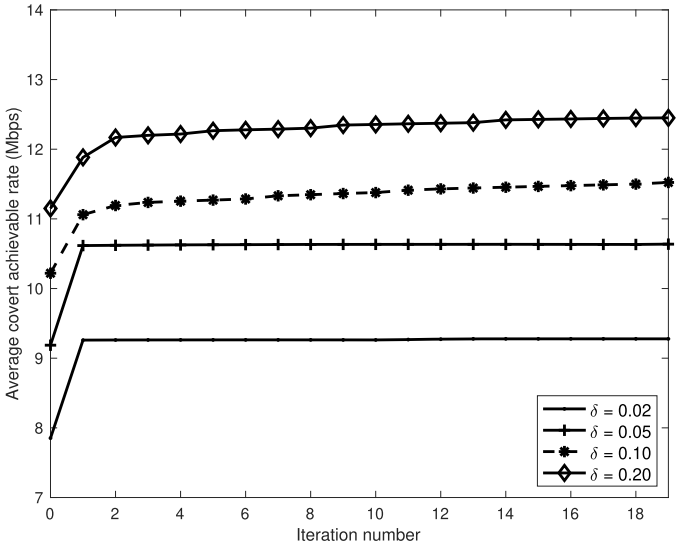

Fig. 2. Convergence of Algorithm 3 for (P0).

Fig. 2 presents the convergence of Algorithm 3 for different DEP thresholds. Specifically, the DEP threshold δ varies from 0.02 to 0.2 and the maximum iterative number is 20. It is observed that after about 5 rounds of iteration, the proposed algorithm converges rapidly to a stationary value. When the DEP threshold δ becomes higher, the average CAR increases by 3.2 Mbps. The reason is that a larger δ leads to a less stringent constraints on covert communications such that the system enjoys a higher flexibility to optimize its resources.

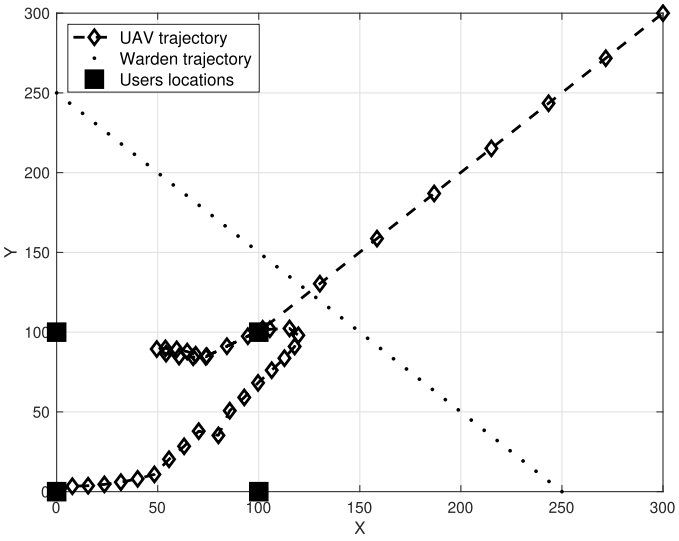

Fig. 3. Projection of the trajectories on the horizontal plane.

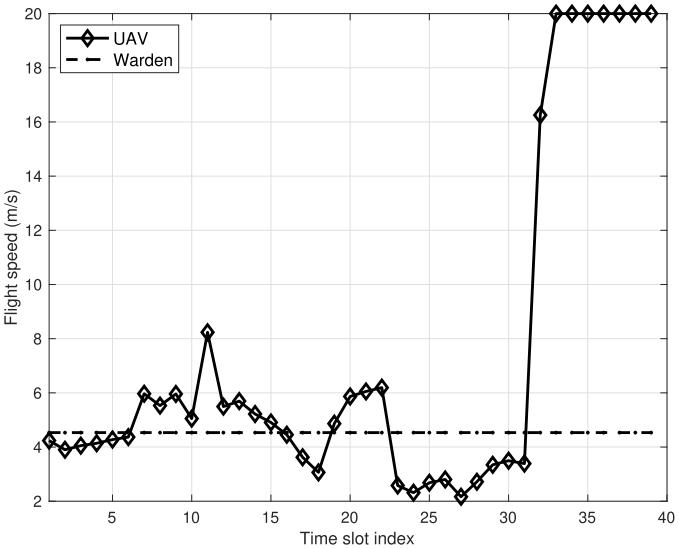

Fig. 4. Flight speeds of the legitimate UAV and the warden UAV.

Fig. 3 shows the projection of the trajectories on the horizontal plane with the default system parameter configurations and Fig. 4 depicts the flight speed of the UAVs. It is observed that the warden UAV flies along a straight line with a uniform speed. We can see that in the initial stage, the legitimate UAV flies quickly to a region near to the ground users. In the second stage, the legitimate UAV circulates around the users. The reason is when the legitimate UAV approaches to the ground users, a stronger signal power from the ground users can be received by the legitimate UAV due to the proximity and the CAR of the ground users is improved. Moreover, when the warden UAV approaches to the legitimate UAV, the latter makes a detour such that its flight direction keeps away from the former. In this scenario, the bottleneck of the covert communication becomes the small distance from the the warden UAV to the legitimate UAV, and the latter tries to stay away from the former while keep as close as possible to the ground users. In the third stage, the legitimate UAV flies to its target point at its full speed.

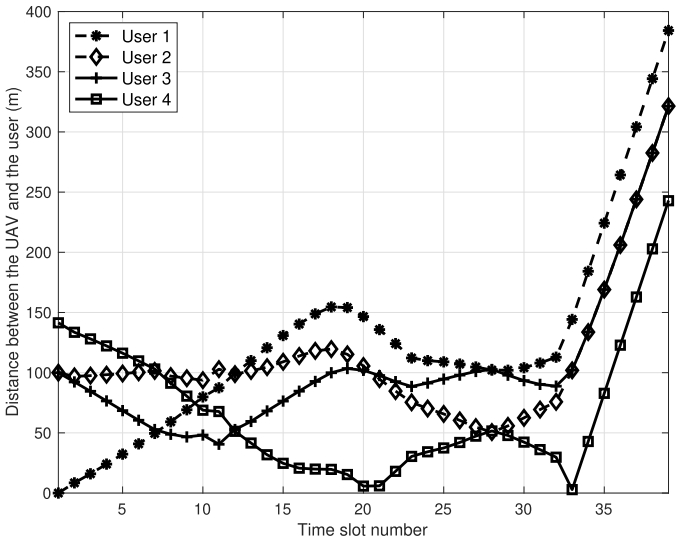

Fig. 5. Distance from the legitimate UAV and all the users.

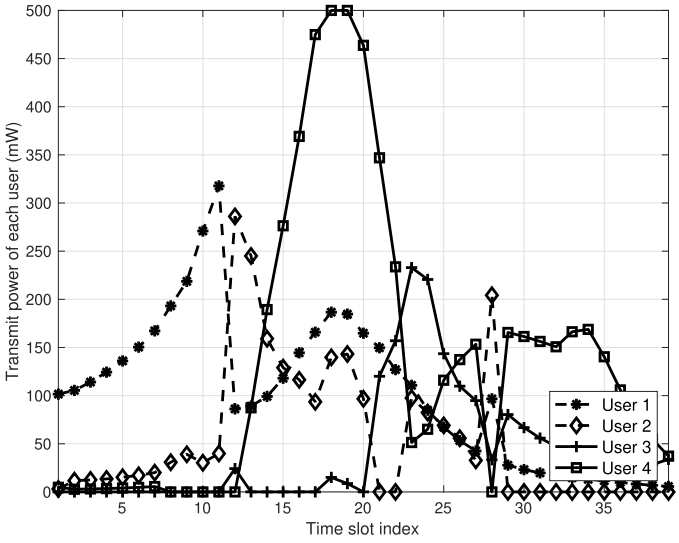

Fig. 6. Transmit power of each user.

Fig. 5 shows the distance from the legitimate UAV and each user, while Fig. 6 shows the corresponding transmit power of each user. We can see from these figures that with the time-varying legitimate UAV position, the distance of

each user varies accordingly. The proposed algorithm adapts the transmit power of each user to achieve the maximum sum CAR. Generally, the nearest user to the legitimate UAV, whose messages are first decoded by the legitimate UAV, may experience much more interference from other user. Thus, more power should be allocated to the nearest user, until the maximum transmit power is reached.

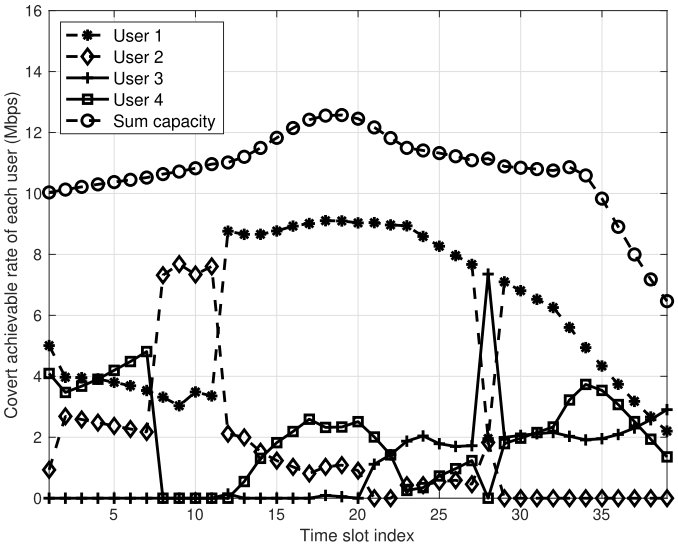

Fig. 7. CAR at each user and sum CAR.

Moreover, the CAR at each user, as well as the sum CAR at each time slot are shown in Fig. 7. Due to different distances from the legitimate UAV, the CAR at each user changes dramatically, whereas the sum CAR remains relatively stable. Specifically, the farthest user, whose messages are last decoded by the legitimate UAV, is not affected by the multi-user interference and therefore achieves the maximum CAR accordingly. Recall that our objective function in (P0) is to maximize the average uplink CAR while guaranteeing a tolerable DEP at the warden UAV. Since the uplink NOMA protocol is adopted, to achieve the maximum average uplink CAR, the transmit power of each user should be coordinated to achieve the maximum uplink sum rate. Thus, some users may have a lower CAR in several time slots compared with the peak CAR.

Fig. 8 shows the projection of the trajectories on the horizontal plane with $K = 2$. Compared with the trajectories of $K = 4$ in Fig. 3, the legitimate UAV spends more time on circulating around the two ground users. The reason is that in order to improve its CAR, the legitimate UAV needs to be closer to the centroid formed by the locations of the users. Since the number of users varies from 4 to 2, the centroid varies from $[50, 50]^T$ to $[50, 0]^T$. Accordingly, the UAV's flight trajectory moves downwards and deviates towards to the X-axis as a whole. When the legitimate UAV circulates around the ground users, a better wireless signal SNR from the ground users can be obtained, and the average CAR is improved.

The impacts of K on the average CAR are shown in Fig. 9, where K varies from 1 to 4. We can see that the average CAR significantly increases with K. Specifically, we can see that the

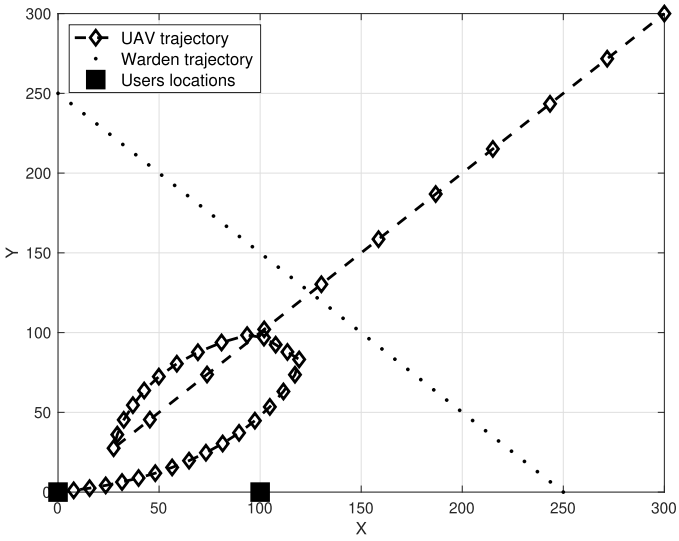

Fig. 8. Projection of the trajectories on the horizontal plane with $K = 2$.

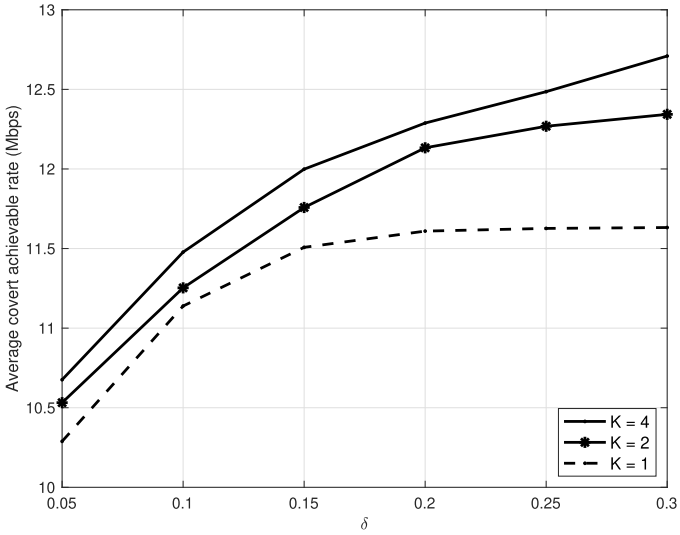

Fig. 9. Average CAR with different users number K.

CAR is increased by 1.2 Mbps when $K = 4$ compared with that of $K = 1$. The reason is that when the number of usersr K becomes larger, more resource allocation freedoms can be obtained by the uplink NOMA protocol. Through optimizing the transmit power of the ground users, the sum CAR can be improved remarkably.

Fig. 10 presents the impacts of the slot number N on the UAV trajectories, where the default parameter settings are adopted while the slot numbers are set as $N = 20$ and $N = 50$, respectively. We can observe that when the slot number N is sufficiently large, the UAV would spend more time on circulating around the target users. The reason is that since N is large, the UAV has enough time to fly to the final position. Thus, more time slots will be spent to be close to the ground users. Consequently, the sum CAR can be improved. Moreover, since the final location of the legitimate UAV is set identically as $\mathbf{c}_{\mathrm{F}} = [300, 300]^T$ in different simulation cases,

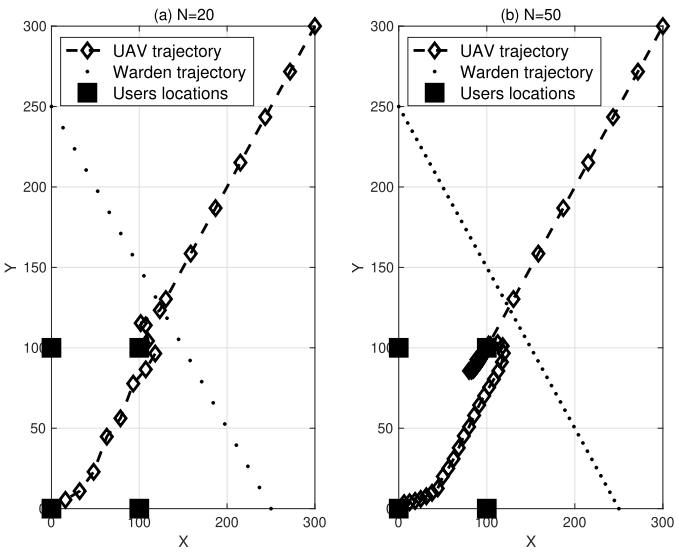

Fig. 10. UAV trajectories with different slot numbers N.

the legitimate UAV always flies to the final location at its fastest speed in the second half of the trajectories. Thus, the second half of the trajectories behave similarly with different slot numbers N.

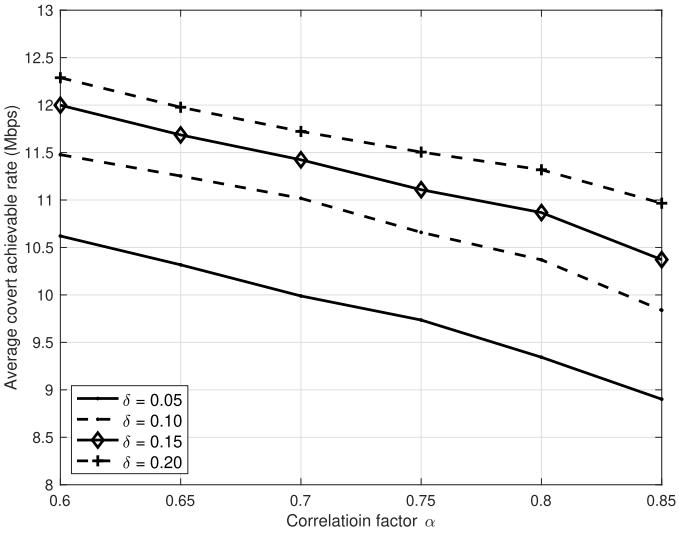

Fig. 11. Average CAR with different correlation factors α.

Fig. 11 presents the impacts of the correlation factor α on the average CAR with different values of the detection thresholds δ. In our simulation, the detection threshold δ varies from 0.20 to 0.05 with a step size of 0.05, and the correlation factor α alters from 0.60 to 0.85. From this figure, we can see that the average CAR decreases with α. According to *Remark* 4, the power radio η^* is monotonically decreasing w.r.t. α. As such, a larger correlation factor α leads to a lower power radio η^*, which strengthens the constraint on the transmit power scheme, and leads to a lower average CAR.

In addition, Fig. 12 shows the impacts of the detection threshold δ and the maximum transmit power of each ground

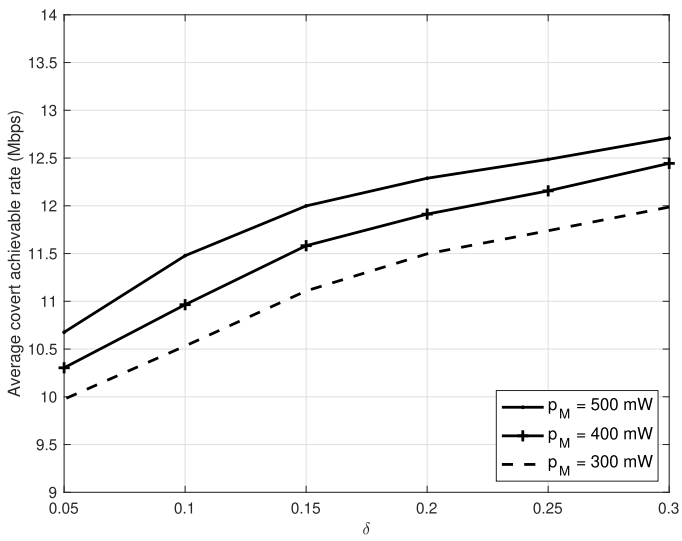

Fig. 12. Average CAR with different DEP thresholds δ.

user p_{M} on the average CAR. In our simulations, p_{L} grows proportionally with p_{M}, and $p_{\mathrm{L}} = 5p_{\mathrm{M}}$. From this figure, we can see that a higher δ is obviously helpful to improve the average CAR. The reason is that according to *Corollary* 1, a higher δ can lead to a lower DEP $P_{\mathrm{E,min}}$, which relaxes the constraint on the power radio η. Thus, a larger average CAR can be achieved. Moreover, with the growth of p_{M}, the average CAR also increases significantly. When p_{M} grows larger, more freedoms of the transmit power for each ground user is granted, therefore, the average CAR can be significantly improved, which is also consistent with expectation.

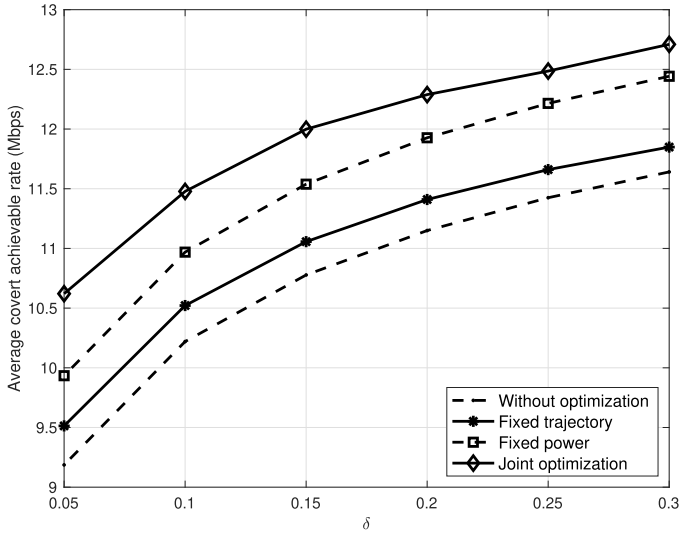

Fig. 13. Performance comparison between different algorithms

Finally, the covertness of the proposed scheme compared with other benchmarks is evaluated in Fig. 13. All of the parameters are set identical to that in Fig. 12, except that the correlation factor is $\alpha = 0.6$, the maximum transmit power of the ground users is $p_{\mathrm{M}} = 200$ mW, and the detection threshold

δ varies from 0.05 to 0.30 with a step size of 0.05. All of the demonstrated algorithms are listed as follows:

1) Without optimization: the legitimate UAV flies along a uniform straight trajectory, while $p_k[n], \forall k$, is set as a constant and uniform value at each time slot;
2) Fixed trajectory: the legitimate UAV flies along a uniform straight trajectory, while the transmit power scheme is optimized as per (P1);
3) Fixed power: the trajectory of the legitimate UAV is optimized as per (P3), while $p_k[n], \forall k$, is set as a constant and uniform value at each time slot;
4) Joint optimization: the proposed joint trajectory and transmit power scheme optimization for (P0) as in Algorithm 3.

From the results, we can observe that the joint optimization scheme outperforms the three benchmarks in terms of the average CAR. Benefiting from the extra degrees of freedom introduced by the trajectory and transmit power optimization, the proposed algorithm can effectively improves the average CAR. In particular, when δ grows larger, the performance gains of the joint optimization algorithm gradually saturated. The reason is that in the region of large δ, the constraint of $P_{\mathrm{E,min}}$ becomes stringent, and the bottleneck of system covert performance becomes p_{M}, that leads to a diminishing return in performance gain compared with the benchmarks.

VI. Conclusion

In this paper, the joint optimization on the UAV trajectory and the transmit power of the ground users was proposed to improve covert communications in UAV-assisted NOMA networks under channel uncertainty. The legitimate UAV transmits the downlink public signals or artificial jamming signals to confuse the detector equipped at the warden UAV, which flies along a predefined trajectory. Along with the optimized trajectory and by adopting the NOMA protocol, the legitimate UAV collects data from multiple ground users simultaneously. To ensure a tolerable DEP at the warden UAV and taking into account the channel estimation uncertainty, we derived the expressions on the optimal normalized detection threshold, the minimum DEP at the warden UAV, and the transmit power constraint for the ground users. Afterwards, we formulated an optimization problem to maximize the average CAR, under the constraints of flight speed, initial and final location, transmit power, and overall DEP. To tackle the formulated non-convex problem, an iterative BCD-based SCA method was proposed to obtain an effective suboptimal solution. In our future work, other application scenarios, such as 3D trajectory optimization for variable flight altitudes, energy-efficient optimization, imperfect CSI, small-scale fading, and mobile ground users, will be investigated.

Appendix A
Proof of Theorem 1

By substituting (15) into (12) and (13) respectively, we have[6]

$$P_{\mathrm{FA}} = \Pr\{u_0 > \hat{\tau} - c_1\} = \begin{cases} 1, & \text{if } \hat{\tau} < c_1, \\ e^{-(\hat{\tau}-c_1)}, & \text{if } \hat{\tau} \geq c_1, \end{cases} \tag{45}$$

and

$$\begin{aligned} P_{\mathrm{MD}} &= \Pr\left\{u_1 < \frac{\hat{\tau}}{1+\eta} - c_1\right\} \\ &= \begin{cases} 0, & \text{if } \hat{\tau} < c_1(1+\eta), \\ 1 - e^{-(\frac{\hat{\tau}}{1+\eta}-c_1)}, & \text{if } \hat{\tau} \geq c_1(1+\eta). \end{cases} \end{aligned} \tag{46}$$

Moreover, substituting (45) and (46) into (14) yields

$$P_{\mathrm{E}} = \begin{cases} 1, & \text{if } \hat{\tau} < c_1, \\ e^{c_1} e^{-\hat{\tau}}, & \text{if } c_1 \leq \hat{\tau} < c_1(1+\eta), \\ 1 - e^{c_1}\left[e^{-\frac{\hat{\tau}}{(1+\eta)}} - e^{-\hat{\tau}}\right], & \text{if } \hat{\tau} \geq c_1(1+\eta). \end{cases} \tag{47}$$

Obviously, P_{E} is a continuous function w.r.t. τ. As for the case of $c_1 \leq \hat{\tau} < c_1(1+\eta)$, P_{E} is strictly monotonically decreasing w.r.t. $\hat{\tau}$. Considering the case of $\hat{\tau} \geq c_1(1+\eta)$, by setting the derivative of P_{E} as zero, i.e., $\frac{\partial P_{\mathrm{E}}}{\partial \hat{\tau}} = 0$, we obtain a stationary point as:

$$\hat{\tau}_0 = \frac{1+\eta}{\eta}\ln(1+\eta). \tag{48}$$

Moreover, if $\hat{\tau} \geq \hat{\tau}_0$, P_{E} is a strictly monotonically increasing function and vice versa. By using the basic inequality of $\ln(1+x) < x$, we have $\frac{\ln(1+\eta)}{\eta} < 1$. On the other hand, for the case of $\alpha \in [0.5, 1)$, we have $c_1 > 1$ and $c_1(1+\eta) > \hat{\tau}_0$. For the case of $\alpha < 0.5$, the optimal value of $P_{E,\mathrm{min}}$ can be achieved at the stationary point $\hat{\tau}_0$. In summary, the optimal threshold can be obtained in (17). Finally, by substituting (17) into (47), we obtain the expressions of the overall DEP as in (18).

Appendix B
Proof of Corollary 1

Given the following definition $W(\eta) = \ln T(\eta)$, applying first-order derivation on $W(\eta)$, yields

$$\frac{\partial W(\eta)}{\partial \eta} = \frac{\ln(1+\eta)}{\eta^2} > 0. \tag{49}$$

Therefore, $W(\eta)$ is a monotonically increasing function w.r.t. η, and so is $T(\eta)$.

Considering the expression of $P_{\mathrm{E,min}}[n]$ in (18), we can prove $P_{\mathrm{E,min}}[n]$ is monotonically decreasing w.r.t. $T(\eta[n])$ and $c_1(\alpha)$, respectively. Since both $T(x)$ and $c_1(\alpha)$ are monotonically increasing functions, $P_{\mathrm{E,min}}[n]$ is monotonically decreasing w.r.t. $\eta[n]$ and α, respectively. As such, *Corollary* 1 is proved.

[6]For the sake of presentation, the time slot index $[n]$ is omitted in this proof.

APPENDIX C
PROOF OF COROLLARY 3

For the case of $\alpha > 0.5$, considering the asymptotic scenario, i.e., $\delta \to 0$, applying the first-order Taylor series expansion on (20), yields

$$\eta^* = \frac{1}{c_1} \ln \frac{1}{1-\delta} = \frac{-1}{c_1} \ln(1-\delta) \to \frac{\delta}{c_1}. \tag{50}$$

Considering the case of $\alpha < 0.5$, we give the following definition

$$U(\eta) = (1+\eta)^{-(1+\frac{1}{\eta})}. \tag{51}$$

Given $\eta \to 0$, using the L'Hospital's rule, yields

$$\lim_{\eta \to 0} \ln U(\eta) = -\lim_{\eta \to 0} \frac{\ln(1+\eta)}{\frac{1}{(1+\frac{1}{\eta})}} = -1. \tag{52}$$

Therefore,

$$\lim_{\eta \to 0} U(\eta) = e^{-1}, \tag{53}$$

and

$$\lim_{\eta \to 0} T(\eta) = \lim_{\eta \to 0} \eta U(\eta) = \eta e^{-1}. \tag{54}$$

Using the original definition of η^* in (20), we have

$$\eta^* \to \delta e^{1-c_1}, \text{if } \alpha < 0.5. \tag{55}$$

Combining (50) and (55), Corollary 3 is proved.

APPENDIX D
PROOF OF LEMMA 1

Applying the first-order derivation on the first function, we obtain

$$\frac{\partial y}{\partial x} = \frac{1}{a + \frac{x}{b}} > 0. \tag{56}$$

Continuing to take the derivative of the above equation, gives

$$\frac{\partial y^2}{\partial^2 x} = -\frac{1}{b(a+\frac{x}{b})^2} < 0. \tag{57}$$

According to the definition of convexity, it is obvious that $\ln(a + \frac{x}{b})$ is concave w.r.t. x. Similarly, by taking second-order derivative of the other function, we obtain

$$\frac{\partial z}{\partial x} = -\frac{b}{ax^2 + bx} < 0, \tag{58}$$

and

$$\frac{\partial z^2}{\partial^2 x} = \frac{(2ax+b)b}{(ax^2+bx)^2} > 0, \tag{59}$$

which proves the convexity of $\ln(a + \frac{b}{x})$ w.r.t. x.

REFERENCES

[1] D. Deng, X. Li, V. Menon, M. J. Piran, H. Chen, and M. A. Janf, "Learning based joint UAV trajectory and power allocation optimization for secure IoT networks," *Digit. Commun. Netw.*, vol. 8, no. 1, pp. 411–418, Nov. 2022.

[2] Bash, Boulat, A., Goeckel, Dennis, Towsley, and Don, "Limits of reliable communication with low probability of detection on AWGN channels," *IEEE J. Select. Areas Commun.*, vol. 31, no. 9, pp. 1921–1930, Sep. 2013.

[3] S. Lee, R. J. Baxley, M. A. Weitnauer, and B. Walkenhorst, "Achieving undetectable communication," *IEEE J. Sel. Top. Sign. Proces.*, vol. 9, no. 7, pp. 1195–1205, Oct. 2015.

[4] B. He, S. Yan, X. Zhou, and V. Lau, "On covert communication with noise uncertainty," *IEEE Commun. Lett.*, vol. 21, no. 4, pp. 941–944, Apr. 2017.

[5] K. Shahzad, X. Zhou, and S. Yan, "Covert communication in fading channels under channel uncertainty," in *2017 IEEE 85th Vehicular Technology Conference (VTC Spring)*, Jun. 2017, pp. 1–5.

[6] J. Hu, S. Yan, X. Zhou, F. Shu, and J. Li, "Covert wireless communications with channel inversion power control in rayleigh fading," *IEEE Trans. Veh. Technol.*, vol. 68, no. 12, pp. 12 135–12 149, Oct. 2019.

[7] R. Ma, X. Yang, G. Pan, X. Guan, Y. Zhang, and W. Yang, "Covert communications with channel inversion power control in the finite blocklength regime," *IEEE Wireless Commun. Lett.*, vol. 10, no. 4, pp. 835–839, Dec. 2021.

[8] Y. Su, H. Sun, Z. Zhang, Z. Lian, Z. Xie, and Y. Wang, "Covert communication with relay selection," *IEEE Wireless Commun. Lett.*, vol. 10, no. 2, pp. 421–425, Oct. 2021.

[9] R. Chen, Z. Li, J. Shi, L. Yang, and J. Hu, "Achieving covert communication in overlay cognitive radio networks," *IEEE Trans. Veh. Technol.*, vol. 69, no. 12, pp. 15 113–15 126, Oct. 2020.

[10] W. Chen, H. Ding, S. Wang, and F. Gong, "On the limits of covert ambient backscatter communications," *IEEE Wireless Commun. Lett.*, vol. 11, no. 2, pp. 308–312, Feb. 2022.

[11] X. Chen, T.-X. Zheng, L. Dong, M. Lin, and J. Yuan, "Enhancing MIMO covert communications via intelligent reflecting surface," *IEEE Wireless Commun. Lett.*, vol. 11, no. 1, pp. 33–37, Jan. 2022.

[12] D. Deng, X. Li, S. Dang, M. C. Gursoy, and A. Nallanathan, "Covert communications in intelligent reflecting surface-assisted two-way relaying networks," *IEEE Trans. Veh. Technol.*, vol. 71, no. 11, pp. 12 380–12 385, Nov. 2022.

[13] C. Wang, Z. Li, J. Shi, and D. W. K. Ng, "Intelligent reflecting surface-assisted multi-antenna covert communications: Joint active and passive beamforming optimization," *IEEE Trans. Commun.*, vol. 69, no. 6, pp. 3984–4000, Jun. 2021.

[14] Y. Li, Y. Zhang, J. Wang, W. Xiang, S. Xiao, L. Chang, and W. Tang, "Performance analysis for covert communications under faster-than-Nyquist signaling," *IEEE Commun. Lett.*, vol. 26, no. 6, pp. 1240–1244, Jun. 2022.

[15] X. Jiang, X. Chen, J. Tang, N. Zhao, X. Y. Zhang, D. Niyato, and K.-K. Wong, "Covert communication in UAV-assisted air-ground networks," *IEEE Wireless Commun.*, vol. 28, no. 4, pp. 190–197, Mar. 2021.

[16] R. Zhang, X. Chen, M. Liu, N. Zhao, X. Wang, and A. Nallanathan, "UAV relay assisted cooperative jamming for covert communications over Rician fading," *IEEE Trans. Veh. Technol.*, vol. 71, no. 7, pp. 7936–7941, Jul. 2022.

[17] H.-M. Wang, Y. Zhang, X. Zhang, and Z. Li, "Secrecy and covert communications against UAV surveillance via multi-hop networks," *IEEE Trans. Commun.*, vol. 68, no. 1, pp. 389–401, Jan. 2020.

[18] J. Zhang, X. Chen, M. Li, and M. Zhao, "Optimized throughput in covert millimeter-wave UAV communications with beam sweeping," *IEEE Wireless Commun. Lett.*, vol. 10, no. 4, pp. 720–724, Apr. 2021.

[19] X. Jiang, Z. Yang, N. Zhao, Y. Chen, Z. Ding, and X. Wang, "Resource allocation and trajectory optimization for UAV-enabled multi-user covert communications," *IEEE Trans. Veh. Technol.*, vol. 70, no. 2, pp. 1989–1994, Feb. 2021.

[20] X. Zhou, S. Yan, D. W. K. Ng, and R. Schober, "Three-dimensional placement and transmit power design for UAV covert communications," *IEEE Trans. Veh. Technol.*, vol. 70, no. 12, pp. 13 424–13 429, Dec. 2021.

[21] X. Zhou, S. Yan, F. Shu, R. Chen, and J. Li, "UAV-enabled covert wireless data collection," *IEEE J. Select. Areas Commun.*, vol. 39, no. 11, pp. 3348–3362, Jun. 2021.

[22] D. Wang, P. Qi, Y. Zhao, C. Li, W. Wu, and Z. Li, "Covert wireless communication with noise uncertainty in space-air-ground integrated

vehicular networks," *IEEE Trans. Intell. Transport. Syst.*, vol. 23, no. 3, pp. 2784–2797, Mar. 2022.
[23] X. Chen, M. Sheng, N. Zhao, W. Xu, and D. Niyato, "UAV-relayed covert communication towards a flying warden," *IEEE Trans. Commun.*, vol. 69, no. 11, pp. 7659–7672, Nov. 2021.
[24] R. Duan, J. Wang, C. Jiang, H. Yao, Y. Ren, and Y. Qian, "Resource allocation for multi-UAV aided IoT NOMA uplink transmission systems," *IEEE Internet Things J.*, vol. 6, no. 4, pp. 7025–7037, Aug. 2019.
[25] Y. Zhang, J. Wang, L. Zhang, Y. Zhang, Q. Li, and K.-C. Chen, "Reliable transmission for NOMA systems with randomly deployed receivers," *IEEE Trans. Comm.*, vol. 71, no. 2, pp. 1179–1192, Feb. 2023.
[26] Q. Li, P. Ren, D. Xu, and Y. Xie, "Covert non-orthogonal multiple access vehicular communications with friendly jamming," in *2020 IEEE Globecom Workshops GC Wkshps*, 2020, pp. 1–6.
[27] Y. Jiang, L. Wang, H. Zhao, and H.-H. Chen, "Covert communications in D2D underlaying cellular networks with power domain NOMA," *IEEE Syst J*, vol. 14, no. 3, pp. 3717–3728, Feb. 2020.
[28] L. Lv, Q. Wu, Z. Li, Z. Ding, N. Al-Dhahir, and J. Chen, "Covert communication in intelligent reflecting surface-assisted NOMA systems: design, analysis, and optimization," *IEEE Trans. Wireless Commun.*, vol. 21, no. 3, pp. 1735–1750, Aug. 2022.
[29] Y. Zhang, W. He, X. Li, H. Peng, K. Rabie, G. Nauryzbayev, B. M. ElHalawany, and M. Zhu, "Covert communication in downlink NOMA systems with channel uncertainty," *IEEE Sensors J.*, vol. 22, no. 19, pp. 19 101–19 112, Oct. 2022.
[30] Z. Hadzi-Velkov, S. Pejoski, and N. Zlatanov, "Achieving near ideal covertness in noma systems with channel inversion power control," *IEEE Commun. Lett.*, vol. 26, no. 11, pp. 2542–2546, Nov. 2022.
[31] M. Wang, W. Yang, X. Lu, C. Hu, B. Liu, and X. Lv, "Channel inversion power control aided covert communications in uplink NOMA systems," *IEEE Wirel. Commun. Lett.*, vol. 11, no. 4, pp. 871–875, Jul. 2022.
[32] L. Tao, W. Yang, X. Lu, M. Wang, and Y. Song, "Achieving covert communication in uplink NOMA systems via energy harvesting jammer," *IEEE Commun. Lett.*, vol. 25, no. 12, pp. 3785–3789, Sep. 2021.
[33] X. Hou, J. Wang, C. Jiang, X. Zhang, Y. Ren, and M. Debbah, "Uav-enabled covert federated learning," *IEEE Trans. Wireless Commun.*, vol. 99, no. 9, pp. 1–1, Early Access, Feb. 2023.
[34] W. Lu, Y. Ding, Y. Gao, Y. Chen, N. Zhao, Z. Ding, and A. Nallanathan, "Secure NOMA-based UAV-MEC network towards a flying eavesdropper," *IEEE Trans. Commun.*, vol. 70, no. 5, pp. 3364–3376, Jan. 2022.
[35] L. Tao, W. Yang, S. Yan, D. Wu, X. Guan, and D. Chen, "Covert communication in downlink noma systems with random transmit power," *IEEE Wireless Commun. Lett.*, vol. 9, no. 11, pp. 2000–2004, Nov. 2020.
[36] Y. Xu, T. Zhang, D. Yang, Y. Liu, and M. Tao, "Joint resource and trajectory optimization for security in UAV-assisted MEC systems," *IEEE Trans. Commun.*, vol. 69, no. 1, pp. 573–588, Jan. 2021.
[37] Y. Zhang, J. Zhang, J. Xiong, L. Zhou, and J. Wei, "Energy-efficient multi-UAV-enabled multiaccess edge computing incorporating NOMA," *IEEE Internet Things J.*, vol. 7, no. 6, pp. 573–588, Jun. 2020.
[38] 3GPP TR 36.777, "Technical specification group radio access network study on enhanced LTE support for aerial vehicles," *IEEE Trans. Veh. Technol.*, vol. 09, no. 1, Jun. 2017.
[39] N. Zhao, X. Pang, Z. Li, Y. Chen, F. Li, Z. Ding, and M. Alouini, "Joint trajectory and precoding optimization for UAV-assisted NOMA networks," *IEEE Trans. Commun.*, vol. 67, no. 5, pp. 3723–3735, Jun. 2019.
[40] T. Yoo and A. Goldsmith, "Capacity and power allocation for fading mimo channels with channel estimation error," *IEEE Trans. Inf. Theory*, vol. 52, no. 5, pp. 2203–2214, Sep. 2006.
[41] L. Musavian, M. R. Nakhai, M. Dohler, and A. H. Aghvami, "Effect of channel uncertainty on the mutual information of MIMO fading channels," *IEEE Trans. Veh. Technol.*, vol. 56, no. 5, pp. 2798–2806, Mar. 2007.
[42] Y. Zhang, W. He, X. Li, H. Peng, K. Rabie, G. Nauryzbayev, B. M. ElHalawany, and M. Zhu, "Covert communication in downlink NOMA systems with channel uncertainty," *IEEE Sensors J.*, vol. 22, no. 19, pp. 19 101–19 112, Oct. 2022.
[43] K. Shahzad, X. Zhou, S. Yan, J. Hu, F. Shu, and J. Li, "Achieving covert wireless communications using a full-duplex receiver," *IEEE Trans. Wireless Commun.*, vol. 17, no. 12, pp. 8517–8530, Dec. 2018.
[44] Y. Zhao, Z. Li, D. Wang, and N. Cheng, "Tradeoffs in covert wireless communication with a controllable full-duplex receiver," *China Commu.*, vol. 19, no. 5, pp. 87–101, Dec. 2021.
[45] Q. Zhang, M. Bakshi, and S. Jaggi, "Covert communication over adversarially jammed channels," *IEEE Trans. Inf. Theory*, vol. 67, no. 9, pp. 6096–6121, July 2021.
[46] M. Grant and S. Boyd, "CVX: Matlab software for disciplined convex programming, version 2.1," http://cvxr.com/cvx, Mar. 2014.
[47] C. You and R. Zhang, "3D trajectory optimization in Rician fading for UAV-enabled data harvesting," *IEEE Trans. Wireless Commun.*, vol. 18, no. 6, pp. 3192–3207, Dec. 2019.
[48] F. Guo, H. Zhang, H. Ji, X. Li, and V. C. Leung, "Joint trajectory and computation offloading optimization for uav-assisted mec with noma," in *IEEE INFOCOM 2019 - IEEE Conference on Computer Communications Workshops (INFOCOM WKSHPS)*, May 2019, pp. 1–6.
[49] Z. Q. Luo, W. K. Ma, M. C. So, Y. Ye, and S. Zhang, "Semidefinite relaxation of quadratic optimization problems," *IEEE Signal Processing Mag.*, vol. 27, no. 3, pp. 20–34, Jun. 2010.